Meteorol. Appl. 10, 301–311 (2003) DOI:10.1017/S1350482703001063

The application of AVHRR data for the detection of volcanic ash in a Volcanic Ash Advisory Centre

S. C. Watkin
Met Office, FitzRoy Road, Exeter, Devon, EX1 3PB, UK
Email: *sarah.watkin@metoffice.com*

A volcanic ash detection product using AVHRR data has been developed for use in the London Volcanic Ash Advisory Centre, operated by forecasters at the Met Office. The product is an image that shows the brightness temperature difference between two infrared channels, which can be used to discriminate between clouds containing volcanic ash particles and those containing water droplets or ice crystals. Factors such as water vapour, water droplet and ice crystal content, opacity, cloud top temperature, ash particle size, surface emissivity properties and instrumental effects all have an effect on the spectral signal represented in the image. AVHRR imagery has been used to study the volcanic clouds ejected from eruptions of Mount Etna (Italy) in July 2001, Hekla (Iceland) in February 2000 and Mount Spurr (USA) in September 1992 to demonstrate the application of this product during volcanic events. The volcanic ash detection product provides essential information that can help forecasters locate volcanic ash and give appropriate guidance through advisory statements to the aviation industry and thus help avoid dangerous and expensive encounters between aircraft and volcanic ash.

1. Background

Volcanic ash in the atmosphere is a significant safety hazard for jet aircraft (Casadevall 1992). The primary cause for concern is the risk of engine shutdown due to the melting of volcanic ash particles within the engine of an aircraft. Volcanic ash particles can also cause extensive damage to the frame and windows of an aircraft by abrasion. Timely and accurate information about the location and extent of volcanic ash can enable a pilot to take evasive action to avoid this hazard (Cantor 1998). There have been numerous aircraft encounters with volcanic ash, some of which have resulted in the activation of emergency procedures to restart engines and large repair costs for aviation companies (Neal et al. 1997; Cantor 1998).

Volcanic Ash Advisory Centres (VAACs) were established in the 1990s in a joint venture between the International Civil Aviation Organisation (ICAO) and the World Meteorological Organisation (WMO). The London VAAC, one of nine VAACs around the world, is operated by the Met Office. Its area of responsibility covers the north-east Atlantic, including Iceland, where 18 volcanoes have been active since AD 1500 (Casadevall & Thompson, 1995). In the event of notification of a volcanic eruption, the role of a VAAC is to run a computer trajectory model, detect and track volcanic ash using satellite imagery, issue advisory information on the extent and forecast trajectory of a volcanic ash cloud and then to monitor the situation and provide regular updates (ICAO 2000). In any one week world-wide, there is usually at least one eruption sufficiently near international air routes to trigger the International Airways Volcano Watch, which includes the activities of VAACs as described above (WMO 1999).

The use of satellite imagery to detect, determine the extent of, and track volcanic ash clouds is discussed in this paper, particularly in relation to the responsibilities of the London VAAC. It discusses the operational practicalities of using Advanced Very High Resolution Radiometer (AVHRR) data to detect volcanic ash. The method used to discriminate between a volcanic ash plume and a water or ice cloud using AVHRR data and the factors that affect the signal in the imagery, reducing the volcanic ash signal or causing false alarms, are described. The benefits of the application of AVHRR data for volcanic ash detection are realised through careful interpretation of the resulting spectral signal represented in the volcanic ash product by forecasters operating the VAAC service.

2. Detection of volcanic ash using AVHRR data

During an explosive eruption the depressurisation of magma causes it to fragment violently forming volcanic ash particles (Simkin 1991). Volcanic ash is just one component of a volcanic cloud. Other components are varying amounts of water vapour, water droplets, sulphuric acid droplets, sulphur dioxide and other gases (Oppenheimer 1998). Here, the term volcanic cloud will be used to describe any cloud containing substances of

volcanic origin and the term volcanic ash cloud will be used to describe a volcanic cloud which is known to contain ash.

The optical properties of volcanic ash particles depend on the composition, size distribution and shape of the particles. Although these properties are not known for particles in a particular volcanic ash cloud when a volcano erupts, studies have shown that volcanic ash particles are generally rich in silica and exhibit stronger absorption at the shorter wavelengths in the 10–12 μm atmospheric window than at the longer wavelengths (Prata 1989a, 1989b). These absorption characteristics are the reverse of those of water vapour and water or ice clouds (Saunders & Kriebel 1988). Prata (1989a) describes a method of using AVHRR data to discriminate between semi-transparent volcanic ash clouds and water or ice clouds. Typically, the difference between the brightness temperature at 10.8 μm ($BT_{10.8}$) and the brightness temperature at 12.0 μm ($BT_{12.0}$) is negative when volcanic ash is present in the atmosphere, and positive when water or ice is present in the atmosphere, such that:

$BT_{10.8} - BT_{12.0} > 0$ for water vapour, water and ice semi-transparent clouds;

$BT_{10.8} - BT_{12.0} < 0$ for semi-transparent clouds containing volcanic ash particles.

In addition to the variation of the optical properties of volcanic ash, the effects of the atmosphere and the Earth's surface on the signal can be strong, affecting the performance of this detection method. Many studies have since been conducted using this technique to observe volcanic ash (e.g. Rose & Mayberry 2000; Constantine et al. 2000; Schneider et al. 1999; Rose et al. 1995).

Satellite data can provide valuable information about the occurrence of a volcanic eruption and about the presence and extent of a volcanic ash cloud. In many remote areas of the world, satellite data may be the only data available to monitor volcanic activity. It is important that the method to detect volcanic ash can be used during both the day and night; therefore a method that uses only thermal infrared radiances is preferable to one that utilises radiances at solar wavelengths. The satellite data used in this study are from the AVHRR instrument on board the NOAA series of polar orbiting satellites. The AVHRR/2 and AVHRR/3 instruments possess channels with the following central wavelengths: 0.6, 0.8, 3.7, 10.8 and 12.0 μm (Kidwell 1998; Goodrum et al. 2000). AVHRR data are used in this study, and operationally at the Met Office, because they have adequate spectral information, spatial resolution (approximately 1.1 km at nadir) and temporal coverage for the high latitudes of the London VAAC area of responsibility (45°N–90°N).

3. Generation of AVHRR-based images for VAAC activities at the Met Office

AVHRR data are routinely received at the Met Office and are processed on the Met Office's 'Autosat' system. The infrared AVHRR 10-bit data are calibrated and converted to brightness temperatures following NOAA guidelines given in Kidwell (1998). This includes a non-linear correction in the conversion of measured counts to radiance to ensure that the brightness temperatures are as accurate as possible since the $BT_{10.8}-BT_{12.0}$ values of interest are small (typically –5 K to +5 K). The data are geolocated and overlaid with a map and grid. An AVHRR $BT_{10.8}-BT_{12.0}$ data array for each of the specified areas is generated and stored as 16-bit data to preserve the high radiometric accuracy of ~0.1 K of the raw AVHRR data. The volcanic ash detection products are converted to images and placed on the Met Office's internal website. These images are accessible to Met Office staff and are available for use by forecasters operating the VAAC service.

AVHRR $BT_{10.8}-BT_{12.0}$ images are generated for two main areas: (1) the north-east Atlantic Ocean (covering the London VAAC area of responsibility) and (2) the Mediterranean area. The latter was chosen to enable forecasters to gain experience from the relatively frequent eruptions of Mount Etna. Typically, 12 to 14 AVHRR $BT_{10.8}-BT_{12.0}$ images that partially cover the London VAAC area of responsibility are currently generated every 24-hour period (with two NOAA polar orbiter satellites in orbit). They are available for forecasters to use within approximately 30 minutes after the radiances were measured.

4. Factors affecting the detection of volcanic ash using $BT_{10.8}-BT_{12.0}$ imagery

The infrared radiation measured by the AVHRR emanates from the earth's surface. This radiation is modified by atmospheric constituents. In cloud-free conditions the $BT_{10.8}-BT_{12.0}$ signal is affected by gaseous absorption, principally due to water vapour, and the properties of the underlying surface. As discussed above, water vapour absorption results in a positive $BT_{10.8}-BT_{12.0}$ signal due to greater absorption at the longer wavelengths in the 10–12 μm atmospheric window. The $BT_{10.8}-BT_{12.0}$ signal over cloud-free surfaces is, in general, small and positive. However, the exceptions are some arid vegetation-free surfaces which can have emissivity properties resulting in a negative $BT_{10.8}-BT_{12.0}$ signal (Ackerman 1997).

In cloudy conditions, the measured $BT_{10.8}-BT_{12.0}$ signal results from a combination of radiation emanating from and modified by the surface, clouds and the intervening atmosphere. The detection technique relies on the differential transmission through the meteorological or volcanic cloud of infrared radiation

emanating from the underlying surface at the two wavelengths (Prata 1989a). Thus, if the cloud is opaque, the signal reaching the satellite instrument originates from the cloud top and the $BT_{10.8}-BT_{12.0}$ signal is close to zero. However, a volcanic ash cloud is usually only opaque soon after it is ejected from the volcano since the concentration of volcanic ash reaches a maximum at the top of the eruption column (Woods & Kienle 1991). The volcanic ash cloud becomes semi-transparent as it entrains ambient air and volcanic ash is deposited downwind of the volcano.

The magnitude of the $BT_{10.8}-BT_{12.0}$ signal is related to the magnitude of the temperature difference between the underlying surface and the cloud top. Wen & Rose (1994) showed that the most negative $BT_{10.8}-BT_{12.0}$ value of a volcanic ash cloud is a linear function of the temperature difference between the underlying surface and the volcanic cloud. Therefore, high altitude volcanic ash clouds, with low cloud-top temperatures, usually result in the largest negative $BT_{10.8}-BT_{12.0}$ values.

The composition, shape and size of volcanic ash particles determine their absorption characteristics and therefore their effect on the measured $BT_{10.8}-BT_{12.0}$ signal. The refractive indices of several samples of volcanic ash (e.g. andesite, basalt, rhyolite) are given in Wen & Rose (1994) and they show the variability in these parameters in wavebands centred at 10.8 μm and 12.0 μm. In general, volcanic ash particles with high silica content cause the strongest negative $BT_{10.8}-BT_{12.0}$ signal. In the 10–12 μm atmospheric window the effect of ash particle shape on the absorption characteristics is negligible compared to the other factors described here (Watkin & Ringer 2000). Therefore the particles can be assumed to be spherical and Mie theory can be used to describe the absorption of radiation.

The mean radius in a size distribution of volcanic ash particles has a large effect on the resulting $BT_{10.8}-BT_{12.0}$ signal. Only particles within the Mie scattering region near the Rayleigh limit exhibit the differential absorption properties at 10.8 μm and 12.0 μm necessary for the application of this detection method (Baran et al. 1993). These particles have radii of approximately 1–15 μm (Constantine et al. 2000). Volcanic ash particles with radii of less than approximately 1 μm, in the Rayleigh scattering regime, have little effect on the measured 10.8 μm and 12.0 μm radiances, resulting in a $BT_{10.8}-BT_{12.0}$ signal that depends mainly on the effects of the atmosphere and the Earth's surface. Volcanic ash particles with radii larger than approximately 15 μm exhibit similar absorption characteristics at 10.8 μm and 12.0 μm, resulting in a near-zero $BT_{10.8}-BT_{12.0}$ signal. C-band radar (with a wavelength of 5 cm) measurements show that particles with diameters greater than 2 mm fall out of suspension within 30 minutes of an eruption (Rose et al. 2000). This rapid decrease in mean particle radii continues with time and means that volcanic ash clouds can be detected using $BT_{10.8}-BT_{12.0}$ imagery soon after an eruption. Indeed, it is the particles of fine ash (with radii of <15 μm) that are most hazardous to aircraft in flight because they can drift for large distances over long periods of time.

Other constituents of volcanic clouds including sulphur dioxide gas, sulphuric acid aerosols, water droplets and ice crystals absorb radiation at infrared wavelengths. Whilst sulphur dioxide has only a narrow absorption band at around 8–9 μm, sulphuric acid aerosol (H_2SO_4) has differential absorption properties in the 10–12 μm atmospheric window which result in a similar $BT_{10.8}-BT_{12.0}$ signal to volcanic ash (Baran et al. 1993). However, the conversion of sulphur dioxide to sulphuric acid is slow, of the order of several days (Baran et al. 1993) depending on altitude, latitude and season, and therefore sulphuric acid aerosol does not affect the detection of volcanic ash in the period immediately following an eruption. Water droplets and ice crystals contribute to a positive $BT_{10.8}-BT_{12.0}$ signal (Saunders & Kriebel 1988). If a volcanic ash cloud contains a large proportion of water droplets and/or ice crystals then the measured $BT_{10.8}-BT_{12.0}$ signal can be positive, masking the volcanic ash signal completely. The water content of a volcanic ash cloud can originate from the magma or from flood water in the crater, but the main origin is thought to be the entrainment of moist air as the volcanic ash cloud rises (Rose et al. 2000). The moist air above and below the volcanic ash cloud also shifts the $BT_{10.8}-BT_{12.0}$ signal in the positive sense. Rose & Prata (1997) found that this shift could be as large as +3 K during a study of an eruption on Montserrat. This is a particular problem in moist tropical atmospheres and for low-level volcanic ash plumes. Volcanic plumes observed at a large viewing angle can also result in a positive $BT_{10.8}-BT_{12.0}$ signal due to the long optical path caused by water vapour absorption; the so-called limb-darkening effect.

A major problem for high-level plumes is that ice crystals can form around the volcanic ash particles, which act as ice condensation nuclei, resulting in a positive $BT_{10.8}-BT_{12.0}$ signal which is representative of a semi-transparent ice cloud. For example, the eruption of Rabual volcano in Papua New Guinea in September 1994 was estimated to contain 2–3 Tg of ice and produced $BT_{10.8}-BT_{12.0}$ values of +3 K to +12 K (Rose et al. 1995).

Volcanic ash can only be successfully discriminated by a forecaster from water or ice cloud using $BT_{10.8}-BT_{12.0}$ imagery if the signal is negative or in a negative sense compared to the background signal. The background signal is the signal from the cloud-free atmosphere in the vicinity of the volcanic ash cloud. The effect on the signal of water in its various states is the largest concern for forecasters interpreting $BT_{10.8}-BT_{12.0}$ imagery.

5. Case studies of volcanic eruptions using AVHRR $BT_{10.8}-BT_{12.0}$ imagery

Presented below are case studies of three different volcanic eruptions. The eruption of Mount Etna in July 2001 sent volcanic ash into the mid-troposphere which was tracked using AVHRR $BT_{10.8}-BT_{12.0}$ imagery generated routinely at the Met Office. In February 2000, Hekla in Iceland erupted producing a stratospheric volcanic cloud which could not be shown to contain volcanic ash using AVHRR $BT_{10.8}-BT_{12.0}$ imagery. Finally the eruption of Mount Spurr in Alaska in September 1992 is presented. This was a large subplinian eruption producing a volcanic ash cloud that could be tracked for over 60 hours in AVHRR $BT_{10.8}-BT_{12.0}$ imagery as it drifted over North America.

5.1. Eruption of Mount Etna in July 2001

Mount Etna is a large continental volcano covering approximately 240 km^2 on the island of Sicily, Italy (37.73°N, 15.00°E). The upper portion of Mount Etna is a stratovolcano which persistently degasses through fissures on the flanks and several craters on the summit (Oppenheimer et al. 1998). The Smithsonian Institution, Global Volcanism Program, describes the events of the eruption which began on 17 July 2001 and continued until 9 or 10 August 2001; these are outlined here. Early on 17 July the first in a series of flank eruptions took place. Over the following days five fissures opened up, four of them new. Lava flowed to within 3 km of the town of Catania, approximately 25 km to the south-east of Mount Etna. On 22 and 23 July 2001, a flank eruption from a fissure at 2.5 km altitude produced a column of volcanic ash estimated to have reached 5.2 km above sea level. The ash cloud drifted in a south-easterly direction covering the area within 25 km with fine ash. Due to the danger to aircraft caused by the volcanic ash, the Fontanarossa International Airport of Catania was closed on 22 July for two days. There were further periods of volcanic ash emissions on 29, 30 July and 2–5 August.

AVHRR $BT_{10.8}-BT_{12.0}$ imagery of the volcanic ash ejected during the eruption of Mount Etna is presented in Figure 1. The imagery is shown for 22 and 23 July 2001, the days when the international airport was closed. The volcanic ash cloud can clearly be seen in the $BT_{10.8}$–$BT_{12.0}$ image on both days. On 22 July at 1243 UTC (Figure 1a) the plume of volcanic ash particles drifted in a south-easterly direction for approximately 650 km. The plume has a width of between 10 and 50 km over most of its length. Although only parts of the plume exhibit negative $BT_{10.8}-BT_{12.0}$ values, with a minimum value of −0.7 K, the rest of the plume visible in this image has $BT_{10.8}-BT_{12.0}$ values which are still less than the surrounding background values allowing the extent of the plume to be determined by a forecaster. The positive areas and the low magnitude negative areas of the volcanic ash plume are probably a result of water vapour absorption in the lower troposphere and/or a low mass loading of volcanic ash particles in the plume. Along the plume there are areas of particularly low $BT_{10.8}-BT_{12.0}$ values. These may be caused by pulsating emissions of volcanic ash from the crater of Mount Etna and therefore show regions of higher mass loading of volcanic ash particles. Within 150 km downwind of the summit of Mount Etna, the regions of negative $BT_{10.8}-BT_{12.0}$ values are at 5 to 20 km intervals. Plume bifurcation (Ernst et al. 1994) occurs approximately 100 km from Mount Etna.

On the following day, 23 July (Figure 1b), the volcanic ash forms a continuous plume extending 200 km in a south-easterly direction which then bifurcates into a southerly and south-easterly drifting plume. The total extent of the plume visible in this image is over 1200 km. The minimum $BT_{10.8}-BT_{12.0}$ value at this time is −1.7 K with the largest magnitude negative $BT_{10.8}-BT_{12.0}$ values within 100 km of the volcano.

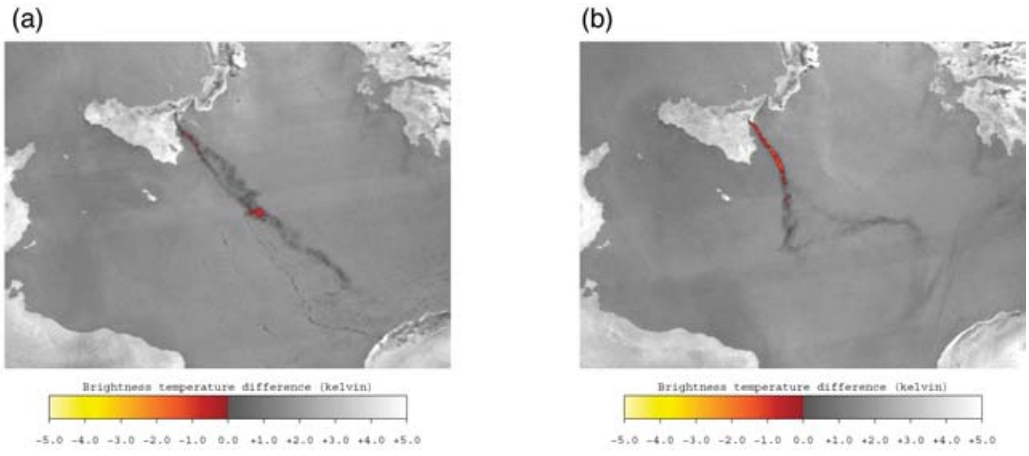

Figure 1. *AVHRR $BT_{10.8}-BT_{12.0}$ images during the eruption of Mount Etna on (a) 22 July 2001 at 1243 UTC and (b) 23 July 2001 at 1252 UTC.*

After drifting for 500 km the plume disperses along a meandering course to the south-east of Sicily.

The area of responsibility for the Toulouse VAAC includes the Mediterranean and therefore the region surrounding Mount Etna. During this period of intense volcanic activity, which resulted in several phases of volcanic ash emissions, the Toulouse VAAC regularly issued volcanic ash advisory statements. The event was also observed by forecasters at the Met Office running the London VAAC service using AVHRR $BT_{10.8}-BT_{12.0}$ imagery. The system to produce these images routinely was put in place in Spring 2001 and so the eruption of Mount Etna in July 2001 provided the first opportunity to observe and interpret this imagery in near real-time during an eruption. Although outside the London VAAC area of responsibility, this event demonstrated how $BT_{10.8}-BT_{12.0}$ images could be used to provide information on the extent of a volcanic ash cloud and therefore aid forecasters in their task of issuing volcanic ash advisory statements.

5.2. Eruption of Hekla in February 2000

Hekla (63.98°N, 19.70°W), a volcano in southern Iceland, started erupting from a 6–7 km long fissure at 1819 UTC on 26 February 2000. The eruption produced a volcanic cloud that was reported to have risen to an altitude of 11 km in only 6 minutes (Smithsonian Institution, Global Volcanism Program). The eruption continued sporadically until 29 February 2000.

Met Office forecasters operating the London VAAC service, which covers the Iceland area, issued over 15 volcanic ash advisory statements during the course of the eruption and during the dispersal of the volcanic cloud. At the time of the eruption, in February 2000, the system to generate AVHRR $BT_{10.8}-BT_{12.0}$ images routinely had not been developed. The information available to the forecasters was from activity reports from Iceland, model output from the Met Office's long-range dispersion model NAME (Ryall & Maryon 1998) and conventional infrared and visible Meteosat and AVHRR imagery.

AVHRR Global Area Coverage (GAC) data were obtained from the NOAA Satellite Active Archive to study the volcanic plume from Hekla retrospectively. GAC data are sub-sampled, averaged values of the instrument field-of-view pixels, which result in an effective spatial resolution at the sub-satellite point of approximately 4 km. The data were calibrated and geolocated following the procedures described by Kidwell (1998) and Goodrum et al. (2000). Figures 2a and 2b show the $BT_{10.8}$ image and the $BT_{10.8}-BT_{12.0}$ image soon after the start of the eruption (the data time of 1806 UTC is the time of the start of this pass). At this time the volcanic cloud was optically thick with a cloud-top temperature of less than 200 K and its

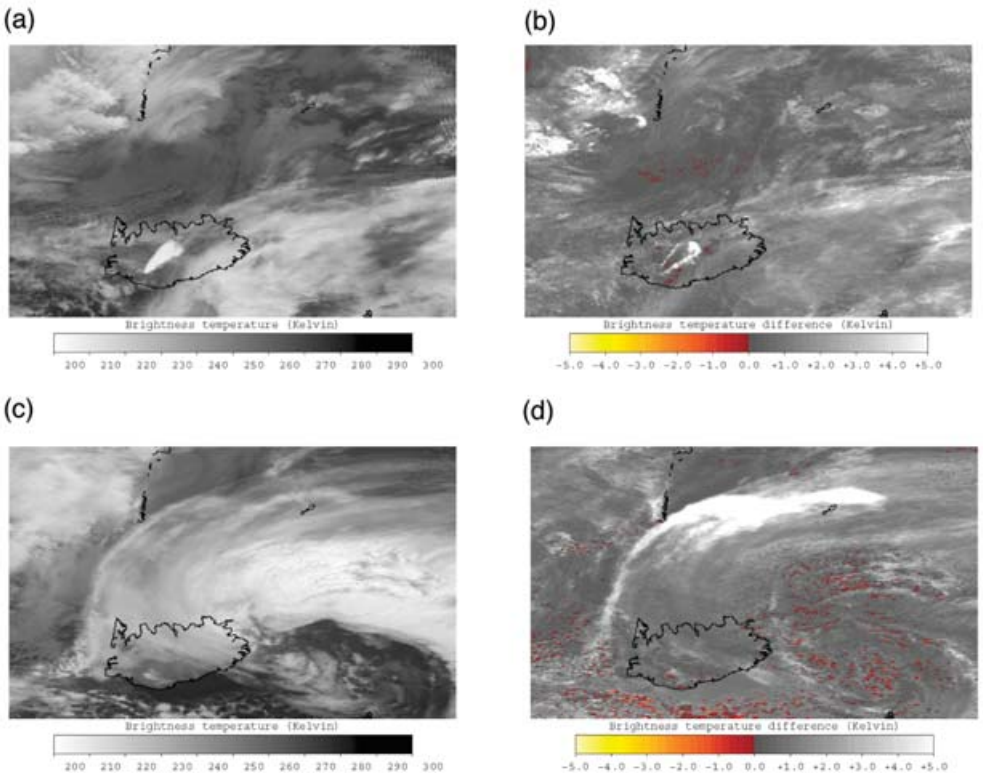

Figure 2. *AVHRR imagery of the volcanic cloud from the eruption of Mount Hekla, Iceland on 26 February 2000. (a) and (b) show the $BT_{10.8}$ and $BT_{10.8}-BT_{12.0}$ images at 1806 UTC on 26 February 2000. (c) and (d) show the $BT_{10.8}$ and $BT_{10.8}-BT_{12.0}$ images at 0552 UTC on 27 February 2000.*

extent could easily be determined. The $BT_{10.8}-BT_{12.0}$ image shows that the volcanic cloud resulted in positive $BT_{10.8}-BT_{12.0}$ values, which are greater than +5 K around the edge. This is indicative of an optically thick ice cloud which is semi-transparent only at its edges. There are no significant negative $BT_{10.8}-BT_{12.0}$ values in this image and therefore volcanic ash cannot be identified using this method.

Figures 2c and 2d show the $BT_{10.8}$ image and the $BT_{10.8}-BT_{12.0}$ image approximately 12 hours later, at 0552 UTC on 27 February 2000. During the previous 12 hours a low-pressure system had moved north over Iceland engulfing the volcanic cloud. At this time the volcanic cloud could not be distinguished from the frontal cloud associated with the low pressure system in the $BT_{10.8}$ image. The $BT_{10.8}-BT_{12.0}$ image shows large positive values to the north of Iceland indicating the presence of semi-transparent ice cloud. However, there are no significant areas of negative $BT_{10.8}-BT_{12.0}$ values that would indicate the presence of volcanic ash. There are some small areas of negative $BT_{10.8}-BT_{12.0}$ values, mainly to the south and east of Iceland; these are caused by instrumental effects and will be discussed later.

Supplementary information was obtained from the retrieval of sulphur dioxide and Aerosol Index from Total Ozone Mapping Spectrometer (TOMS) UV data. These data (not shown), produced by the TOMS SO2 and Ash Group, based at the NASA Goddard Space Flight Center, indicate that the eruption of Hekla produced a significant amount of sulphur dioxide, of up to 30 Dobson units compared to a background level of 10–14 Dobson units. The Aerosol Index is a measure of the difference between measured and simulated ratios of reflected radiances at two ultra-violet wavelengths (Torres et al. 1998). It is affected by the type of aerosol and the particle size distribution. In this case, the Aerosol Index indicated that there was an abundance of sulphate aerosol aligned with the high concentrations of sulphur dioxide and coincident with the semi-transparent ice cloud apparent in the AVHRR $BT_{10.8}-BT_{12.0}$ image on 27 February 2000.

The eruption of Hekla in February 2000 produced a volcanic cloud with a high sulphur dioxide content which over time generated sulphate aerosols. The volcanic cloud resulted in high positive $BT_{10.8}-BT_{12.0}$ values indicating the presence of semi-transparent ice cloud. Rose et al. (2001a) suggest that the sulphate aerosol acted as cloud condensation nuclei to facilitate the growth of ice cloud. The $BT_{10.8}-BT_{12.0}$ images and the TOMS retrieved Aerosol Index do not indicate the presence of volcanic ash particles. However, volcanic ash was reported to have fallen 300 km to the north of Hekla (Smithsonian Institution, Global Volcanism Program) and there is some evidence that silicate-based material, not conclusively from Hekla, was ingested into the engine of a NASA research aircraft that flew through the path of the volcanic cloud from Hekla (Rose et al. 2001a). The ash fall indicates that there were some coarse ash particles in the eruption cloud, but that rapid sedimentation resulted in a short life-time in the volcanic cloud. As described above, the $BT_{10.8}-BT_{12.0}$ imagery cannot be used to detect coarse ash particles (greater than approximately 15 μm in diameter). The resulting evidence about the presence of volcanic ash in the volcanic cloud is unclear and this case illustrates the need for careful interpretation of the AVHRR $BT_{10.8}-BT_{12.0}$ imagery by forecasters and an understanding of the factors that can affect the signal during a volcanic event.

5.3. Eruption of Mount Spurr in September 1992

Mount Spurr (61.30°N, 152.25°W) is a stratovolcano in Alaska which erupted between approximately 0630 UTC and 0900 UTC on 17 September 1992 (Smithsonian Institution, Global Volcanism Program). Radar data from the National Weather Service in the USA indicated that the volcanic plume, containing coarse volcanic ash particles (2–20 mm in diameter (Rose et al. 2001b), reached an altitude of 13.5–15.0 km at approximately 1000 UTC (Smithsonian Institution, Global Volcanism Program). Rose et al. (2001b) give a full description of the three eruptions of Mount Spurr during 1992.

AVHRR GAC data were obtained from the NOAA Satellite Active Archive covering the period 17–20 September 1992. The data were calibrated and geolocated following the procedures described by Kidwell (1998). Figure 3 shows AVHRR $BT_{10.8}-BT_{12.0}$ images on three successive days in which the volcanic ash cloud is clearly visible. The first image (Figure 3a) shows the volcanic ash cloud approximately 600 km to the south-east of Mount Spurr. The ash drifted in a south-south-easterly direction over the Canadian/United States border (Figure 3b), covering a distance of approximately 3000 km in 30 hours. Minimum $BT_{10.8}-BT_{12.0}$ values of −8.3 K occurred at this time. The final image (Figure 3c) shows the elongated volcanic ash cloud stretching from Lake Michigan to the Hudson Strait, a distance of over 2000 km. At this time, when the ash cloud was approximately 52 hours old, a minimum $BT_{10.8}-BT_{12.0}$ value of −19.2 K was recorded in the centre of the distal ash cloud. The largest negative values are likely to be collocated with a part of the semi-transparent ash cloud that has a high concentration of volcanic ash particles, low concentration of water vapour and low atmospheric water vapour content above (i.e. at high altitude). The ash cloud was still visible in the final AVHRR $BT_{10.8}-BT_{12.0}$ image 66 hours after the eruption.

The minimum $BT_{10.8}-BT_{12.0}$ values observed for this volcanic ash cloud are particularly low, down to −19.2 K. The high altitude of this volcanic ash cloud, into the stratosphere, results in a large temperature difference between the surface and the cloud top

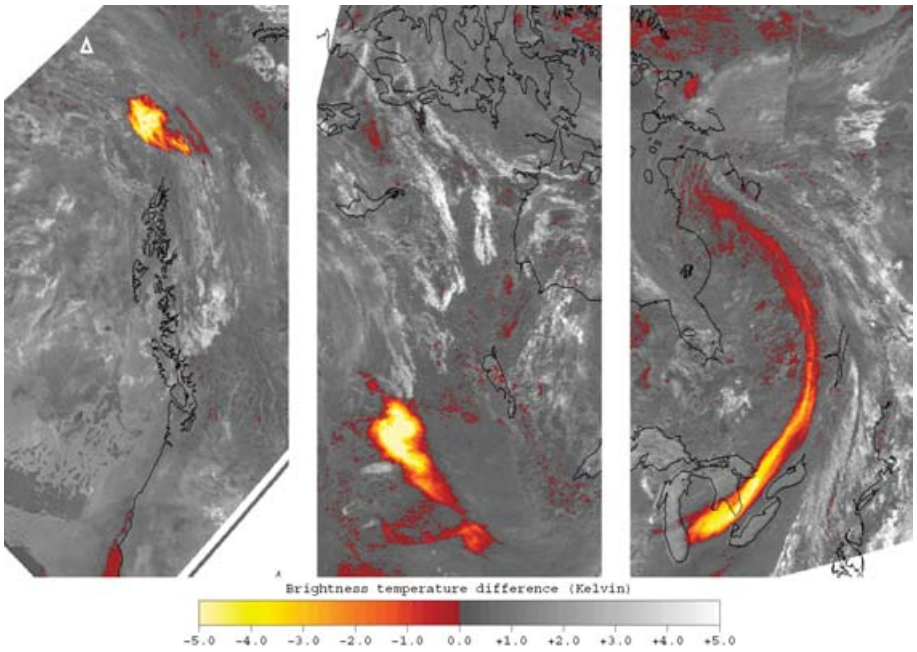

Figure 3. *AVHRR $BT_{10.8}-BT_{12.0}$ images of the volcanic ash cloud from the eruption of Mount Spurr, Alaska, on 17 September 1992 at (a) 1531 UTC on 17 September 1992, (b) 1321 UTC on 18 September 1992 and (c) 1250 UTC on 19 September 1992. The white triangle in (a) marks the location of Mount Spurr.*

(estimated to be >66 K, using figures in Rose et al. 2001b), and the rapid rise of the eruption column through air with a low water vapour content to a high altitude leads to a volcanic ash cloud with a low ice content. These are major factors that contribute to the particularly low $BT_{10.8}-BT_{12.0}$ values observed.

This series of AVHRR $BT_{10.8}-BT_{12.0}$ images demonstrates how this imagery may be used to track a volcanic ash cloud over a period of time from a single eruption. The images provide invaluable information for VAAC forecasters on the presence and extent of volcanic ash and they can be used to verify forecast dispersion model output on the dispersal of a volcanic ash cloud.

6. False alarms in AVHRR $BT_{10.8}-BT_{12.0}$ imagery

In order to use $BT_{10.8}-BT_{12.0}$ imagery operationally it is necessary to understand and recognise situations that can cause negative $BT_{10.8}-BT_{12.0}$ signals without volcanic ash being present in the atmosphere. Such situations include the presence of mineral dust in the atmosphere, some cloud-free non-vegetated surfaces, misalignment between the two AVHRR channels and data calibration errors.

6.1. Mineral dust

Atmospheric constituents which have similar optical properties to volcanic ash will produce a similar $BT_{10.8}$–$BT_{12.0}$ signal. Mineral dust particles originating from the weathering of non-vegetated surfaces commonly contain silica and therefore have similar optical properties to volcanic ash. Ackerman (1997) reports that negative $BT_{10.8}$–$BT_{12.0}$ values are observed to occur for dust storms over the Arabian Peninsula, Africa and the south-west United States. Monitoring of the routinely produced AVHRR $BT_{10.8}$–$BT_{12.0}$ imagery at the Met Office shows that negative values due to mineral dust clouds originating from the Sahara occur occasionally over the coast of North Africa and over the Mediterranean Sea. However, mineral dust particles may also be a hazard to aircraft. Their abrasive nature and high silica content that may damage aircraft in a similar way to volcanic ash particles.

Figure 4a shows an area of negative $BT_{10.8}$–$BT_{12.0}$ values over the Algerian coast on 25 August 2000. Other satellite imagery and derived products from SeaWiFs, Meteosat, TOMS and MODIS (not shown) all indicate that the cause of these negative $BT_{10.8}$–$BT_{12.0}$ values is mineral dust from North Africa. Whilst mineral dust clouds can resemble volcanic ash clouds, they infrequently drift to high latitudes and cause false alarms in the London VAAC area of responsibility. However, they have the potential to be mis-classified as a volcanic ash cloud in the tropical and sub-tropical regions in which they tend to be generated and disperse (Husar et al. 1997). Information from a trajectory model can assist in determining whether the area of negative $BT_{10.8}$–$BT_{12.0}$ values originated from a volcano or a mineral dust source (Simpson et al. 2003).

6.2. Non-vegetated surfaces

In clear sky situations and with negligible atmospheric absorption, the satellite-measured radiances depend

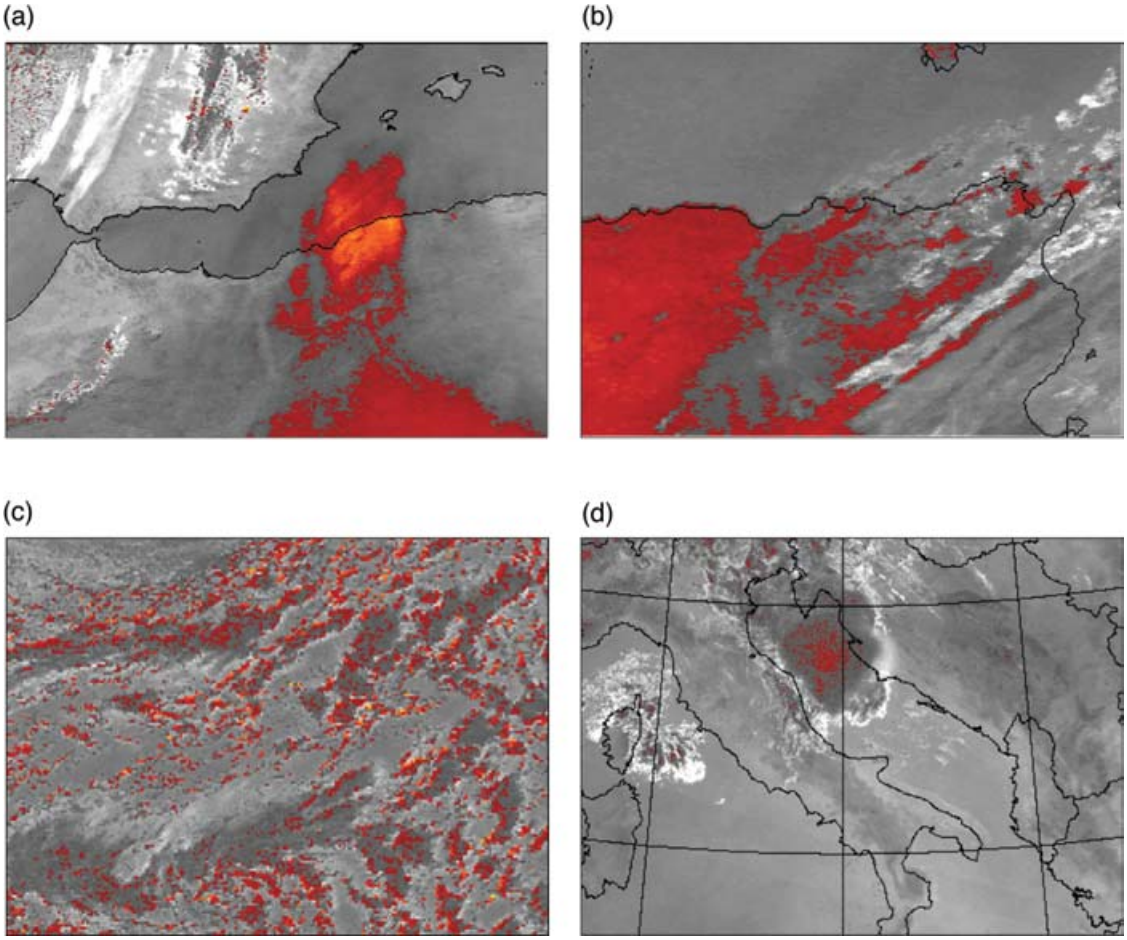

Figure 4. *AVHRR $BT_{10.8}-BT_{12.0}$ imagery showing examples of situations which can cause negative values without volcanic ash being present in the atmosphere. (a) mineral dust over the Algerian coast, (b) cloud-free desert in North Africa, (c) misalignment between channels AVHRR 4 and 5, and (d) high altitude clouds with low cloud top temperatures. See Figure 1 for the coloured key to the brightness temperature difference values presented here.*

only on the surface characteristics. Soils with high quartz content have emissivities which can lead to a negative $BT_{10.8}$–$BT_{12.0}$ signal under these conditions (Prata 1989a; Ackerman 1997). Figure 4b shows AVHRR $BT_{10.8}$–$BT_{12.0}$ imagery with negative values over cloud-free areas of North Africa. Although these regions of negative $BT_{10.8}$–$BT_{12.0}$ may resemble volcanic ash clouds in some circumstances, they are unlikely to be identified as such by a forecaster since volcanic ash clouds would result in lower infrared brightness temperatures than cloud-free areas.

6.3. Interchannel misalignment

Misalignment between AVHRR 10.8 μm and 12.0 μm channels can cause negative $BT_{10.8}$–$BT_{12.0}$ values to occur over inhomogeneous scenes. When the two channels are misaligned, each channel measures radiation emanating from a slightly different scene. Only over inhomogeneous areas where individual fields of view can contain regions with different brightness temperatures can negative (and positive) $BT_{10.8}$–$BT_{12.0}$ values be caused by the misalignment between the channels. Differences in the angular size of the field of view between each channel also contributes to non-zero $BT_{10.8}$–$BT_{12.0}$ values.

Plots of the centre of the fields of view for each AVHRR instruments on NOAA 12, 14, 15 and 16 were obtained from the National Climatic Data Center, NOAA, and the angular sizes of the fields of view from Kidwell (1998) and Goodwin et al. (2000). Assuming negligible atmospheric absorption, surface and cloud emissivities of unity and a square field of view for the AVHRR 10.8 μm and 12.0 μm channels, $BT_{10.8}$–$BT_{12.0}$ values were computed for varying cloud fractions. The radiance for each channel is given by:

$$I = (1 - A)B(T_S) + (A)B(T_C),$$

where A is the cloud fraction in the field of view, T_S is the surface temperature, T_C is the cloud-top height and $B(T)$ is the Planck radiance. $BT_{10.8}$–$BT_{12.0}$ is computed by inverting the Planck function for the radiance simulated for each channel and subtracting the

Table 1. *Angular size and misalignment values for the 10.8 μm and 12.0 μm channels on four AVHRR instruments on the NOAA series of satellites. The minimum $BT_{10.8}-BT_{12.0}$ values were calculated assuming negligible atmospheric absorption, surface and cloud emissivities of unity and a square field of view. The cloud fraction was varied (in steps of 0.1) in the 10.8 μm field of view and the corresponding cloud fraction calculated for the 12.0 μm channel. The $BT_{10.8}-BT_{12.0}$ value was calculated for a surface temperature of 285 K and a cloud-top temperature of 235 K. Channel misalignment values were obtained from the National Climatic Data Center, NOAA and angular sizes of the fields of view from Kidwell (1998) and Goodwin et al. (2000).*

	Field of view (mrad)			
NOAA	10.8 μm	12.0 μm	Misalignment (mrad)	Minimum $BT_{10.8}-BT_{12.0}$ (K)
12	1.41	1.3	0.016	− 1.8
14	1.41	1.3	0.037	− 2.3
15	1.3	1.3	0.059	− 2.9
16	1.3	1.3	0.031	− 1.5

brightness temperatures. The minimum $BT_{10.8}$–$BT_{12.0}$ values for AVHRR instruments on NOAA 12, 14, 15 and 16 are presented in Table 1.

These computations demonstrate that the misalignment between the 10.8 μm and 12.0 μm channels on AVHRR can cause negative $BT_{10.8}$–$BT_{12.0}$ values of a similar magnitude to those caused by volcanic ash. However, the spatial distribution of negative $BT_{10.8}$–$BT_{12.0}$ values caused by channel misalignment is different from that for volcanic ash. Figure 4c shows a $BT_{10.8}$–$BT_{12.0}$ image containing negative values along the edges of cumulus clouds. The pattern formed in the $BT_{10.8}$–$BT_{12.0}$ imagery is of clusters of small distinct areas of negative values. This is quite different from the continuous area of negative $BT_{10.8}$–$BT_{12.0}$ values seen for volcanic ash and therefore an experienced forecaster can recognise a false alarm of this nature.

6.4. High altitude clouds with low cloud-top temperatures

Potts & Ebert (1996) describe how negative $BT_{10.8}$–$BT_{12.0}$ values can occur over tropical areas of Asia when no ash particles are present but there is deep convection and associated cold cloud tops. Figure 4d shows a $BT_{10.8}$–$BT_{12.0}$ image containing negative values collocated with particularly low $BT_{10.8}$ values of down to 211 K over the Adriatic Sea. Potts & Ebert (1996) showed that the negative $BT_{10.8}$–$BT_{12.0}$ values can partially be explained by a failure to account correctly for the non-linear response of the AVHRR infrared sensors at cold temperatures. Deep convective clouds that overshoot the tropopause can also cause negative $BT_{10.8}$–$BT_{12.0}$ values. Due to the temperature inversion that exists at this altitude, the radiation at 10.8 μm emanates from a cooler level than the 12.0 μm radiation (Potts & Ebert 1996). However, inspection of the $BT_{10.8}$–$BT_{12.0}$ and $BT_{10.8}$ images in this situation shows that the negative values correspond to the opaque region of the convective cloud and the semi-transparent region of the cloud, around the edges, indicates that the cloud is composed of ice crystals rather than volcanic ash.

7. Discussion

The presence of volcanic ash particles in the atmosphere poses a threat to aircraft safety. As the number of flights increases and as flight routes expand into remote or as yet undeveloped areas so the risk of jet aircraft encountering volcanic ash clouds increases. This highlights the necessity of developing and applying techniques to detect and determine the extent of a volcanic ash cloud. The use of AVHRR satellite imagery for this purpose has been recognised for some time.

It has been shown how AVHRR data can be used operationally by forecasters running VAAC services. Volcanic eruptions are relatively rare compared with most meteorological events that forecasters deal with routinely. Therefore, regular rehearsals and revision of the use of AVHRR imagery are necessary to ensure that the imagery can be interpreted and used to its maximum potential in the event of a volcanic eruption or the presence of a volcanic ash cloud within the VAAC area of responsibility. To use this imagery effectively the factors that affect the signal in $BT_{10.8}$–$BT_{12.0}$ imagery need to be understood. The main factors are: water vapour, water droplet and ice crystal content, opacity, cloud-top temperature, ash particle size, surface emissivity properties and instrument effects.

Satellite imagery is one source of information that forecasters have available to them in the event of volcanic activity. Other information may come from pilot reports, surface-based observations and output from a dispersion model. However, all of these rely on information being passed to the VAAC from external sources. Satellite imagery is routinely available to VAAC forecasters and covers regions that are not covered by other sources of observation. As the application of satellite data develops and the limitations of the data are better understood the importance of these data for the detection of volcanic eruptions and subsequent tracking of volcanic ash should increase.

A new generation of multi-spectral imagers offers the opportunity to build on the application of AVHRR imagery for the detection of volcanic ash. The Spinning Enhanced Visible and Infrared Radiometer (SEVIRI) on the Meteosat Second Generation (MSG) series of geostationary satellites will measure radiances in

12 spectral channels every 15 minutes from a geostationary position of zero degrees longitude. Data from SEVIRI will provide a large volume of spectral information at high temporal frequency which should enable a volcanic ash detection system to deliver accurate information about the presence of volcanic ash within the MSG field of view quickly to VAAC forecasters. Development of such a system is underway at the Met Office.

Acknowledgements

The author wishes to express her gratitude to Met Office colleagues who have helped in this work. In particular, to the Satellite Systems and Products Group in the Met Office who have implemented and maintained the routine generation of the volcanic ash product and have obtained some of the AVHRR data for the studies presented in this paper. Also, to Dr B. J. Conway and Dr J. R. Eyre for their support, guidance and helpful review of this paper.

References

Ackerman, S. A. (1997) Remote sensing of aerosols using satellite infrared observations. *J. Geophys. Res*. **102**: 17069–17079.

Baran, A. J., Foot, J. S. & Dibben, P. C. (1993) Satellite detection of volcanic sulphuric acid aerosol. *Geophys. Res. Lett*. **20**: 1799–1801.

Cantor, R. (1998) Complete avoidance of volcanic ash is the only procedure that guarantees flight safety. *ICAO J*. **53**: 18–19.

Casadevall, T. J. (1992) Volcanic hazards and aviation safety. *Federal Aviation Administration Aviation Safety J*. **2**: 9–17.

Casadevall, T. J. & Thompson, T. B. (1995) World map of volcanoes and principal aeronautical features. *Geophysical Investigations Series (US Geological Survey)*.

Constantine, E. K., Bluth, G. J. S. & Rose, W. I. (2000) TOMS and AVHRR observations of drifting volcanic clouds from the August 1991 eruptions of Cerro Hudson. In P. Mouginis-Mark, J. Crisp, J. & J. Fink (eds.), *Remote Sensing of Active Volcanism*, AGU Monograph **116**: 45–64.

Ernst, G. G. J., Davis, J. P. & Sparks, R. S. J. (1994) Bifurcation of volcanic plumes in a crosswind. *Bull. Volcanology* **56**: 159–169.

Goodrum, G., Kidwell, K. B. & Winston, W. (eds.) (2000) *NOAA KLM User's Guide*. National Oceanic and Atmospheric Administration.

Husar, R. B., Prospero, J. M. & Stowe, L. L. (1997) Characterisation of tropospheric aerosols over the oceans with the NOAA advanced very high resolution radiometer optical thickness operational product. *J. Geophys. Res*. **102**: 16889–16909.

ICAO (2000) *Handbook on the International Airways Volcano Watch: Operational Procedures and Contact List*. International Civil Aviation Organisation.

Kidwell, K. B. (ed.) (1998) *NOAA Polar Orbiter Data User's Guide (TIROS-N, NOAA-6, NOAA-7, NOAA-8, NOAA-9, NOAA-10, NOAA-11, NOAA-12, NOAA-13 and NOAA-14)*. National Oceanic and Atmospheric Administration.

Neal, C. A., Casadevall, T. J., Miller, T. P., Hendley II, J. W. & Stauffer, P. H. (1997) Volcanic ash—danger to aircraft in the North Pacific. *US Geological Survey Fact Sheet* 030-97.

Oppenheimer, C. (1998) Volcanological applications of meteorological satellites. *Int. J. Remote Sensing* **19**: 2829–2864.

Potts, R. J. & Ebert, E. E. (1996) On the detection of volcanic ash in NOAA AVHRR infrared satellite imagery. *Proceedings of the 8th Australian Remote Sensing Conference*.

Prata, A. J. (1989a) Observations of volcanic ash clouds in the 10–12 μm window using AVHRR/2 data. *Int. J. Remote Sensing* **10**: 751–761.

Prata, A. J. (1989b) Infrared radiative transfer calculations for volcanic ash clouds. *Geophys. Res. Lett*. **16(11)**: 1293–1296.

Rose, W. I. & Mayberry, G. C. (2000) Use of GOES thermal infrared imagery for eruptive scale measurements, Soufrière Hills, Montserrat. *Geophys. Res. Lett*. **27**: 3097–3100.

Rose, W. I. & Prata, A. J. (1997) Atmospheric corrections for two band infrared volcanic cloud discriminations and retrievals. *EOS Trans. AGU, Fall Meet. Suppl*. Abstract F818.

Rose, W. I., Delene, D. J., Schneider, D. J., Bluth, G. J. S, Krueger, A. J., Sprod, I., McKee, C., Davies, H. L. & Ernst, G. G. J. (1995) Ice in the 1994 Rabaul eruption cloud: implications for volcano hazard and atmospheric effects. *Nature* **375**: 477–479.

Rose, W. I., Bluth, G. J. S. & Ernst, G. G. J. (2000) Integrating retrievals of volcanic cloud characteristics from satellite remote sensors: a summary. *Phil. Trans. R. Soc. Lond. A*.

Rose, W. I., Bluth, G., Riley, C., Watson, M., Yu, T. & Ernst, G. G. (2001a) Potential mitigation of volcanic cloud hazards using satellite data: a case study of the February 2000 Hekla event and an unexpected NASA DC8 encounter. *EOS Trans. AGU, 82(47), Fall Meet. Suppl*. Abstract V32F-01.

Rose, W. I., Bluth, G. J. S., Schneider, D. J., Ernst, G. G. J., Riley, C. M., Henderson, L. J. & McGimsey, R. G. (2001b) Observations of volcanic clouds in their first few days of atmospheric residence: the 1992 eruptions of Crater Peak, Mount Spurr Volcano, Alaska. *J. Geology* **109**: 677–694.

Ryall, D. B. & Maryon, R. H. (1998) Validation of the UK Met. Office's NAME model against the ETEX dataset. *Atmospheric Environment* **32**: 4265–4276.

Saunders, R. W. & Kriebel, K. T. (1988) An improved method for detecting clear sky and cloudy radiances from AVHRR data. *Int. J. Remote Sensing* **9**: 123–150.

Schneider, D. J., Rose, W. I., Coke, L. R., Bluth, G. J. S., Sprod, I. & Krueger, A. J. (1999) The first four days of volcano/atmosphere interaction following a stratospheric eruption as observed with TOMS and AVHRR. *J. Geophys. Res*. **104**: 1037–1050.

Simkin, T. (1991) Volcanoes: their occurrence and geography. *Volcanic Ash and Aviation Safety: Proceedings of the First International Symposium on Volcanic Ash and Aviation Safety*, 75–78.

Simpson, J. J., Hufford, G. L., Servranckx, R., Berg, J. & Pieri, D. (2003) Airborne Asian Dust: Case study of long-range transport and implication for the detection of volcanic ash. *Wea. & Forecasting* **18**: 121–141.

Torres, O., Bhartia, P. K., Herman, J. R., Ahmad, Z. & Gleason, J. (1998) Derivation of aerosol properties from satellite measurements of backscattered ultraviolet radiation: theoretical basis. *J. Geophys. Res*. **103**: 17099–17110.

Watkin, S. C. & Ringer, M. A. (2000) Investigation into the use of SEVIRI imagery for the automatic detection of volcanic ash clouds. Met Office FR Tech. Rep. No. 297. Unpublished report available from the National Meteorological Library, London Road, Bracknell, RG12 2SZ, UK.

Wen, S. & Rose, W. I. (1994) Retrieval of sizes and total masses of particles in volcanic clouds using AVHRR bands 4 and 5. *J. Geophys. Res*. **99**: 5421–5431.

WMO (1999) *Implementation Aspects of the World Area Forecast System: the ICAO International Airways Volcano Watch*. Commission for Aeronautical Meteorology (Eleventh Session), Doc. 6.

Woods, A. W. & Kienle, J. (1991) The injection of volcanic ash into the atmosphere. *Volcanic Ash and Aviation Safety: Proceedings of the First International Symposium on Volcanic Ash and Aviation Safety*, 101–106.